JACS
JOURNAL OF THE AMERICAN CHEMICAL SOCIETY
Article
pubs.acs.org/JACS

Isomer-Selected Photoelectron Spectroscopy of Isolated DNA Oligonucleotides: Phosphate and Nucleobase Deprotonation at High Negative Charge States

Matthias Vonderach,[†] Oli T. Ehrler,[†] Katerina Matheis,[†] Patrick Weis,[†] and Manfred M. Kappes*[,†,‡]

[†]Institute of Physical Chemistry, and [‡]Institute of Nanotechnology, Karlsruhe Institute of Technology (KIT), 76128 Karlsruhe, Germany

Supporting Information

ABSTRACT: Fractionation according to ion mobility and mass-to-charge ratio has been used to select individual isomers of deprotonated DNA oligonucleotide multianions for subsequent isomer-resolved photoelectron spectroscopy (PES) in the gas phase. Isomer-resolved PE spectra have been recorded for tetranucleotides, pentanucleotides, and hexanucleotides. These were studied primarily in their highest accessible negative charge states (3−, 4−, and 5−, respectively), as provided by electrospraying from room temperature solutions. In particular, the PE spectra obtained for pentanucleotide tetraanions show evidence for two coexisting classes of gas-phase isomeric structures. We suggest that these two classes comprise: (i) species with excess electrons localized exclusively at deprotonated phosphate backbone sites and (ii) species with at least one deprotonated base (in addition to several deprotonated phosphates). By permuting the sequence of bases in various $[A_{5-x}T_x]^{4-}$ and $[GT_4]^{4-}$ pentanucleotides, we have established that the second type of isomer is most likely to occur if the deprotonated base is located at the first or last position in the sequence. We have used a combination of molecular mechanics and semiempirical calculations together with a simple electrostatic model to explore the photodetachment mechanism underlying our photoelectron spectra. Comparison of predicted to measured photoelectron spectra suggests that a significant fraction of the detected electrons originates from the DNA bases (both deprotonated and neutral).

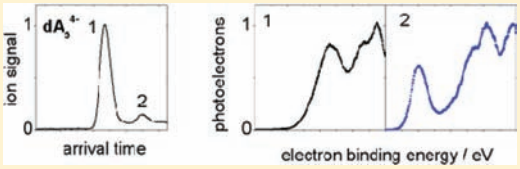

1. INTRODUCTION

Driven primarily by applications in sequencing, studies of DNA by mass spectrometric methods have become ubiquitous.[1−16] As a result, the structural motifs of single- and double-stranded DNA ions isolated in the gas phase have become of great interest. Small, single-stranded oligonucleotides,[17−20] duplexes,[21−23] hairpins,[24] and quadruplexes,[25−27] as well as telomeric sequences,[28,29] have been investigated. H/D exchange,[30−32] blackbody radiation induced dissociation (BIRD),[33,34] ion mobility spectrometry,[35,36] and laser photodissociation[37−40] are among the experimental methods that have been used to obtain such structural information. Often these approaches have also allowed insight into the isomer distributions pertaining, albeit without so far allowing isomer specific spectroscopic probes of the components. Below we report an extensive isomer-resolved spectroscopic study of DNA oligonucleotide ions isolated in the gas phase.

In pH neutral solution, the phosphate backbone of single-stranded oligomeric DNA is usually deprotonated, and the ensuing localized negative charges are surrounded by counterions, also reflecting charge shielding by the solvent. Electrospray ionization (ESI) is the general technique to transfer such molecules from solution into the gas phase, typically resulting in (partially) deprotonated, multiply charged anions completely free of solvent molecules but often with some attached counterions (typically sodium). For a given oligonucleotide sequence dN_x (where N represents the nucleobases adenine (A), cytosine (C), guanine (G), and thymine (T)), standard electrospray conditions yield a range of different charge states, with $(x-1)^-$ the highest negative charge state typically attainable, corresponding to the number of phosphates in the backbone. Such $[dN_x-(x-1)H]^{(x-1)-}$ species are $(x-1)$-fold deprotonated relative to the neutral, undissociated oligonucleotide. In contrast to their lower charged congeners, gas-phase $[dN_x-(x-1)H]^{(x-1)-}$ species typically do not manifest (sodium) counterion complexation. For simplicity, we will generally abbreviate them as $dN_x^{(x-1)-}$ in the following text.

Chen et al.[41] have estimated the gas-phase acidities (GPA) of the nucleic bases by combining experimental data on dissociation and photoelectron spectra of negatively charged bases generated by electron impact. They obtained experimental as well as theoretical values that are close to the GPA of phosphoric acid dimethyl ester.[42] The latter is in turn thought to have a GPA similar to that of the phosphate group of DNA. Therefore, in contrast to aqueous solutions for which nucleobase deprotonation becomes appreciable only at extremely high pH, it is conceivable that highly charged DNA oligonucleotide multianions isolated in the gas phase could manifest both phosphate and nucleobase deprotonation. We explore this below.

Received: January 19, 2012
Published: April 23, 2012

Gas-phase structures of multiply charged anions can be very sensitive to the positions of localized charges and the distances between them. Conversely, to correctly describe the structures of such species, it is necessary to know the exact position of the (excess) charges. This kind of information is also relevant for an understanding of optical response, both static and dynamic. One approach to obtain information on the positions of localized charges in isolated DNA oligonucleotide multianions is photoelectron spectroscopy (PES). Several years ago, we reported the first such measurements. Specifically, we observed that (isomer mixtures of) dA_5^{4-} and dT_5^{4-} had quite different, that is, strongly base-dependent, PES spectra.[43] Shortly afterward, a PES study of singly charged mono- and small oligonucleotides ($dNMP^-$ and dN_x^- (x = 2,3)) provided insight into the underlying photodetachment mechanism.[44] In the case of $dGMP^-$, evidence for the threshold photodetachment of electrons from the (neutral) guanine base was observed, whereas only detachment from phosphate groups was seen for the other $dNMP^-$ species studied (N = A, C, and T). Also, lower adiabatic detachment energies (ADE) were observed for di- and trinucleotide monoanions containing G, than for sequences without G, suggesting more facile photodetachment from (neutral) G also for the former sequences. A subsequent study of the UV photodepletion cross sections of dN_6^{3-} together with electronic structure calculations showing that HOMO and HOMO−1 orbitals were localized over the aromatic portions of the nucleobases provided further support for photodetachment from bases.[39]

We have recently shown that a powerful method to study the localization of charges in large isolated molecular multianions subject to multiple coexisting structures is to combine ion mobility spectrometry and mass spectrometry (IMS-MS; for preselection by collision cross section and mass-to-charge ratio) with negative ion PES.[45] This allows separately determining the electronic signature of each resolvable gas phase conformation/isomer. We demonstrated the first combination of IMS with PES using dC_6^{5-} as a test case. This ionic species manifests four separable gas-phase structures, which do not interconvert under room-temperature conditions on a mass spectrometric time scale. Interestingly, our isomer-resolved PE spectra showed a strong dependence on the collision cross section and thus on the geometric structure of the selected isomer. In particular, we observed that the species with largest collision cross section had the smallest ADE, which is counterintuitive in a purely electrostatic repulsion picture, suggesting that various types of localized excess charge distributions might pertain. In the present study, we further explore, generalize, and attempt to rationalize these observations focusing on a range of isolated, single-stranded DNA oligonucleotides at highest achievable negative charge states, $x - 1$. To reduce complexity as far as possible, we have studied the shortest sequences for which detachment thresholds were still accessible to our experimental setup (the shorter is the $dN_x^{(x-1)-}$ oligonucleotide, the higher is typically the ADE). Correspondingly, we have obtained mass and conformer resolved PES spectra of all poly-N dN_4^{3-}, dN_5^{4-}, and dN_6^{5-}. Additionally, we have carried out IMS-PES measurements for several other oligonucleotides, which incorporate base substitutions or phosphate functionalizations, to learn more about the positions of the localized charges. We report these measurements below together with force-field and semiempirical quantum chemical calculations on dN_5^{4-}, which were used to explore the initial states of the photodetachment process. Together, the data obtained suggest that at the $x - 1$ charge states accessed, structures with exclusively deprotonated phosphates can often coexist with structures having one or more deprotonated bases. These two types of "charge isomer" do not spontaneously interconvert on the experimental time scale under gas-phase conditions (at room temperature). However, their relative abundance can be changed by collisional excitation upon ion injection into the IMS.

2. EXPERIMENTAL METHODS

The oligonucleotides used in this work were obtained from Jena Bioscience and were used without further purification. They were dissolved in water/methanol (1:4 ratio, concentration 0.1 mM) and transferred into the gas phase by electrospray ionization. The experiments were performed in a home-built ESI-IMS-MS-PES instrument, which has been described in detail previously.[45] Briefly, the sprayed oligonucleotides were guided by an hourglass ion-funnel,[46] which also acts as an ion trap, thus allowing one to transform the continuous ion current generated by the ESI source into ion packets for pulsed injection into the drift tube. In this work, the voltage of the injection plate (and thus the injection energy of ions into the drift tube) was varied over a range of 50−100 V so as to facilitate collision-induced heating to generate as many different isomers/conformers of the investigated oligonucleotides as possible. As was already reported in earlier studies,[30,45] raising the injection energy also had an effect on the relative abundances of resolvable isomers, indicating that they can be converted from one structure into another by collisional excitation. Typically, preferential transformation into the isomer having the largest collision cross section was observed.

After injection into the 60 cm long, helium filled (2.5−3 mbar) drift tube held at room temperature, ions were separated in time by the application of a homogeneous electric drift field (typically 10 V/cm, resolving power $t/\Delta t \approx 40$ at the 4^- charge state). From the measured drift times, we determined the corresponding ion mobilities K_0 usually normalized to 298 K and a pressure of 1.013 bar. Ion mobilities can be directly converted to collision cross sections Ω using eq 1:

$$K_0 = \frac{3q}{16N_0}\sqrt{\frac{2\pi}{\mu k_B T}}\frac{1}{\Omega} \quad (1)$$

Here, q is the charge of the ion, N_0 is the number density, T is the temperature of the collision gas, and μ is the reduced mass as calculated for the ion and the helium collision partner.

Ions leaving the drift tube were focused through an exit ion funnel. They subsequently passed a quadrupole ion guide, were turned by a 90° ion mirror, and were finally separated according to their mass-to-charge ratio using an on-axis quadrupole mass filter (Extrel), which was typically set to a mass resolution of $m/\Delta m \geq 100$. Note that, in a number of cases, higher resolution ($m/\Delta m \geq 10000$) mass spectra of sample solutions were separately acquired using an LTQ XL ETD Orbitrap mass spectrometer (Thermo Scientific) under electrospray conditions similar to those used for the IMS-PES measurements, to check the extent of sodiation at the negative charge states probed. A corresponding mass spectrum of a dA_5 solution obtained under conditions optimized for dA_5^{4-} signal is shown in the Supporting Information (Figure S1). This indicates that sodiated species (i.e., $d(A_5-5H+Na)^{4-}$) were not present in measurable amounts for the $(x - 1)^-$ charge state. Analogous observations were made for all of the other cases probed.

After quadrupole mass filtering, ions were then refocused by a stack of electrostatic lenses before passing into the detachment chamber of a time-of-flight photoelectron spectrometer. The photoelectron spectrometer is of the magnetic bottle type, based on the design by Kruit and Read.[47,48] Typically, the fourth harmonic (266 nm) of a Nd:YAG was used for photodetachment. For some measurements, we also used the fifth harmonic (213 nm). Photoelectron spectra were integrated over 200 000 laser shots at a resolution of ~3% ($\Delta E_{kin}/E_{kin}$). To compensate for background electrons coming from scattered light hitting metal surfaces, the laser was run at twice the frequency of the pulsed ion beam. For each photoelectron spectrum, we also recorded

dx.doi.org/10.1021/ja300619j | J. Am. Chem. Soc. 2012, 134, 7830−7841

an alternate shot reference spectrum (laser on, ion beam off) and subtracted both spectra from each other. Selection of the proper arrival time of the desired mass-selected and isomer/conformer-separated ions in the PES spectrometer was achieved by adjusting the temporal delay between ion injection into the drift cell and laser pulse.

Kinetic energies E_{kin} of photodetached electrons were determined by measuring the flight time to the detector. From these, the electron binding energies (EBE) were determined using Einsteiń s photoelectric equation (EBE = $h\nu - E_{kin}$). The adiabatic electron affinity (AEA) corresponds to the EBE of the most weakly bound electron and can be estimated by linearization of the rising flank of the PES spectrum (and extrapolation to the baseline). In the following, we refer to the number obtained by this procedure as the adiabatic detachment energy (ADE). Also subject in detail to the specific signal-to-noise of the corresponding measurements, ADEs reported below are typically accurate to ±0.2 eV. The vertical detachment energy (VDE) corresponds to the energy required to generate the $(n - 1)^-$ charge state (in its ground electronic state) at the same geometry as that of the initial n^- charge state. We assign the VDE to the first maximum in the corresponding PES spectrum. For other details concerning calibration and transformation procedures followed, see ref 45.

Note that for several of the DNA oligonucleotide multianions studied here, we have observed negative ADEs and VDEs.[43,45] Electronic metastability on a mass spectrometric time-scale is a well-known phenomenon associated with many kinds of multianions; for example, $[CuPc(SO_3)_4]^{4-}$ has an ADE of −0.9 eV.[49,50] Under collisionless conditions, electronically metastable multianions decay by electron tunnelling autodetachment from their ground states. The associated lifetimes can be on the order of seconds depending on the system and its vibrational excitation. Higher vibrational excitation levels, for example, as a result of collisions, lead to more rapid tunnelling. Therefore, experimental setups that subject multianions to more extensive collisional excitation prior to their PES are less sensitive toward the species with more negative ADEs; these will be preferentially lost or not detected at all. In the setup used here, we begin to observe such effects for $dN_x^{(x-1)-}$ having ADEs < −1.0 eV.

3. COMPUTATIONAL METHODS

The AMBER program package[51] was used to generate multiple candidate structures for the oligonucleotides of interest. We illustrate the procedures used by describing the homopentanucleotide calculations. First, an otherwise random structure having a preconceived charge distribution was built. For every pentanucleotide ion, three different charge isomer types were tested: (i) class A, an isomer in which all four phosphate groups were deprotonated; (ii) class B − an isomer having three deprotonated phosphate groups and a base deprotonated at the most acidic position of the given

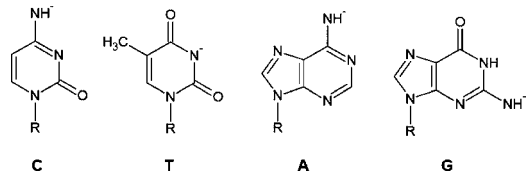

Figure 1. Deprotonated DNA base structures as used for the calculations; see section 3 (C = cytosine, T = thymine, A = adenine, and G = guanine).

heterocycle (as shown in Figure 1),[41] and finally (iii) class C, a species for which three phosphate groups as well as a hydroxyl group at the 5-end were deprotonated. For the charge isomers with a deprotonated base, we also systematically varied which base was deprotonated along the sequence.

Upon generating the starting geometries, these were used for further simulated annealing cycles with the AMBER force field. In this way, we generated 1000 structures each for dA_5^{4-} and dG_5^{4-} as well as 500 structures for dC_5^{4-} and dT_5^{4-}, respectively. Collision cross sections were calculated for every such structure using the angle averaged projection model.[52,53] To obtain accurate energetic data that allow a comparison of the different charge isomer classes, the semiempirical method PM6[54] (implemented in the MOPAC program package) was then utilized to calculate the total, respectively, the HOMO energy, of every structure (see Supporting Information, Figure S2). Afterward, preferred structures were picked out by using the following procedure. First, structures having collision cross sections that differed by more than ±5% from the experimental ones were eliminated (assuming that the isomers with the highest experimental electron binding energies can be assigned to class A candidate structures having all phosphate groups deprotonated; see below). The remaining structures were then sorted according to their absolute PM6 energies. Finally, the average values (total energy, HOMO energy, and collision cross section) of the 50 lowest energy structures of dA_5^{4-}/dG_5^{4-} and the 25 lowest energy structures of dC_5^{4-}/dT_5^{4-} were calculated for each charge isomer type. Note that among the charge isomers having one deprotonated base (class B), extensive simulated annealing cycles were only carried out for those structures with deprotonated terminal bases as preliminary calculations had shown that varying the base deprotonation position in the sequence yields similar total energies.

Concerning the averaging procedure used, several comments are in order. Beyond "dividing" the dN_5^{4-} trial geometries into three different charge isomer types (A, B, and C), we did not further subdivide into classes having a common geometry. The three groups of charge isomers over which the averages were determined always contained the most stable geometry found for that particular charge isomer class. To check that the averages obtained do not depend dramatically on the selection conditions, a sensitivity analysis was also performed in which the accepted collision cross section range and total number of lowest energy structures were independently varied (from ±3 to ±7% and from 20 to 80, respectively). This had no effect on the conclusions (see below).

4. RESULTS AND DISCUSSION

4.1. Isomer Structure-Resolved Photoelectron Spectra. *4.1.1. Tetranucleotide Trianions: dA_4^{3-}, dC_4^{3-}, dG_4^{3-}, and dT_4^{3-}.* Figure 2 shows PES spectra obtained at a detachment wavelength of 266 nm for all resolvable isomers/conformers of the triply charged (homo)tetranucleotides. There are up to three resolvable isomers apparent in the corresponding arrival time distributions (ATDs) shown on the left-hand side of the figure. This ATD panel also introduces the isomer numbering system used (from smallest to largest collision cross section).

For dT_4^{3-}, only one isomer is observed in the ion arrival time distributions (ATD). The PES spectrum indicates an ADE of 2.5 eV. For dA_4^{3-}, two isomers can be resolved. The smaller collision cross section isomer $dA_4^{3-}(1)$ shows a broad band centered at around 2.5 eV and an ADE of 1.3 eV. The PES spectrum of $dA_4^{3-}(2)$ indicates a similar ADE (1.4 eV).

The ion arrival time distribution of dG_4^{3-} shows at least three different features, which we assign to several conformers/isomers. The first feature (1) with the lowest drift time looks asymmetric, implying that the corresponding photoelectron spectrum (1) probably involves at least two overlapping isomers. At later arrival times (and correspondingly larger collision cross sections), a lower intensity structure (2) and then a stronger well-resolved structure (3) are observed. The PES spectra of (1) and (2) each show a wide band at an electron binding energy around 2.5 eV and a long tail toward smaller binding energies (corresponding to an ADE of approximately 1.5 eV). We also observe a wide PES band around 2.5 eV for structure (3). The corresponding ADE (3) at ca. 2 eV is somewhat higher than for those (1) and (2).

dx.doi.org/10.1021/ja300619j | J. Am. Chem. Soc. 2012, 134, 7830−7841

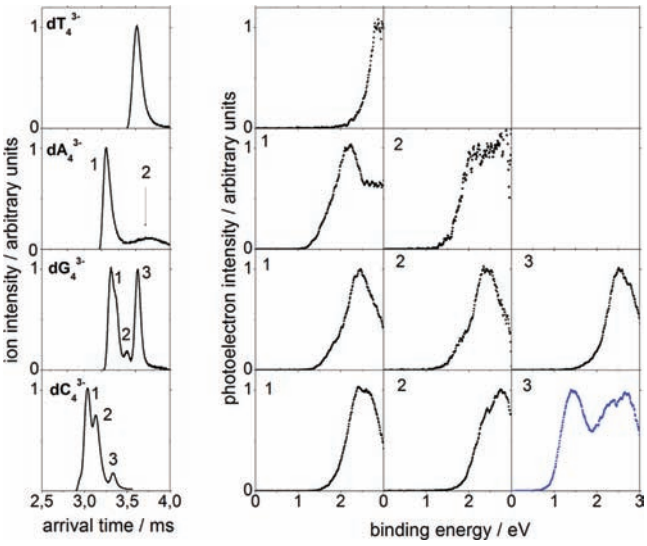

Figure 2. Ion arrival time distributions (ATD, left) and isomer resolved photoelectron spectra (PES, right) obtained at a detachment wavelength of 266 nm for the triply negatively charged homotetranucleotides. Numbers refer to different isomers in order of elution as resolved by ion mobility differences, and probed by PES. Note the blue curve for the largest $dC_4^{3-}(3)$ isomer indicating an electronic structure that differs significantly (lower ADE and more structured spectrum) from those of all other tetranucleotide trianions probed.

In the case of dC_4^{3-}, like dG_4^{3-}, we can again resolve three different structures by IMS. However, while the PES spectra of structures $dC_4^{3-}(1)$ and $dC_4^{3-}(2)$ are again very similar, the third isomer/conformer of $dC_4^{3-}(3)$ has a significantly different PES spectrum with a new well-separated band at much lower binding energies. Note that $dC_4^{3-}(3)$ has a larger collision cross section than the other two isomers. Correspondingly, the average spatial separation between the three phosphate groups would be expected to be larger for this isomer, if indeed the phosphates carry all of the excess negative charges. The repulsive Coulomb interaction between excess charges in multianions decreases their (local) binding energy. Therefore, lower Coulomb repulsions as associated with larger charge separations should lead to (relatively) larger electron binding energies. Why then is the electron binding energy of isomer (3) significantly lower than that of the other conformers?

The extent to which the electron binding energy at a given photoemission site is reduced by interaction with localized excess charges can be estimated as the sum of the Coulomb interactions between outgoing electron and all (other) localized excess charges in the molecule, n, eq 2.[55,43]

$$\mathrm{VDE}^{m-} = \mathrm{VDE} - \sum_{i=1}^{n} \frac{e^2}{4\pi\varepsilon_0\sigma}\frac{1}{r_i} \qquad (2)$$

Here, r_i is the respective distance between the excess charges and the (initially) localized photoemitted electron, m is the total number of excess electrons in the multianion, VDE is the electron binding energy at the photoemission site in the absence of surrounding localized excess charges, and σ is a dielectric shielding constant. For the purposes of this study, which studies highly charged species, we estimate σ to be 1.

Assuming that the three excess charges of $dC_4^{3-}(1)$ and $dC_4^{3-}(2)$ are each localized on the deprotonated phosphates, we conclude that at least one of the deprotonation sites of $dC_4^{3-}(3)$ must be elsewhere and associated with a significantly lower (local) electron affinity. In dC_4^{3-}, the energetically next most favorable positions for deprotonation (after phosphate) are either: (i) the C4 amino group of the cytosine nucleobase (leading to excess negative charge delocalization over the π-system of the base) or (ii) the hydroxyl groups on the desoxyribose at the beginning or end of the oligonucleotide chain.

4.1.2. Nucleobase or Sugar Deprotonation in $dC_4^{3-}(3)$? To explore whether in fact nucleobases or hydroxyls are deprotonated in highly charged oligonucleotide anions, we next sprayed a derivative of dC_4, comprising phosphate groups attached to both terminal hydroxyl groups (=P–dC_4–P, see Figure 3). If base deprotonation were also to occur in this derivative, the corresponding PES spectrum should look similar to that of $dC_4^{3-}(3)$. If a hydroxyl sugar is deprotonated in $dC_4^{3-}(3)$, this would not be possible in the "phosphate

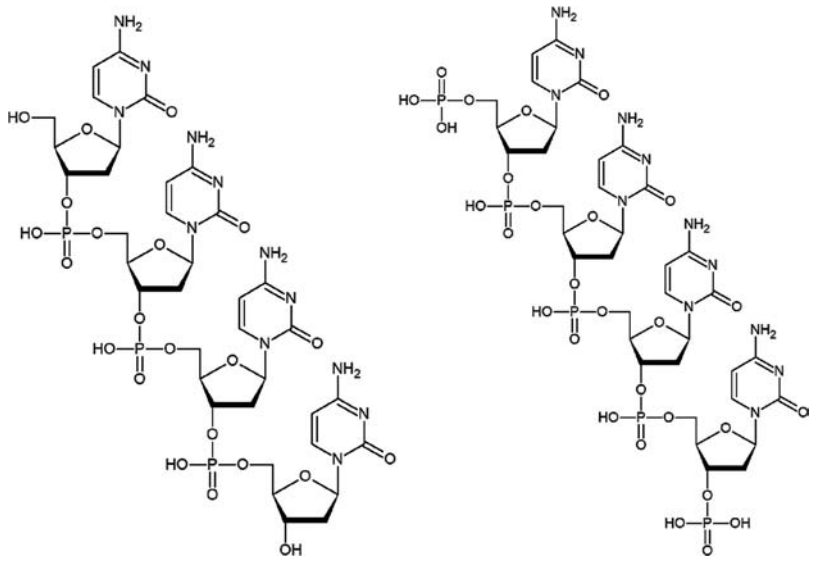

Figure 3. Schematic representations of neutral dC_4 (left) and of the corresponding P–dC_4–P derivative (right). In the latter, phosphate groups have been attached to the hydroxyl groups at the beginning and end of the dC_4 sequence.

dx.doi.org/10.1021/ja300619j | J. Am. Chem. Soc. 2012, 134, 7830–7841

protected" P−dC$_4$−P derivative, and there should be no corresponding similarity.

Figure 4 shows the arrival time distributions and PES spectra of P−dC$_4$−P in the triply and quadruply negative charge states.

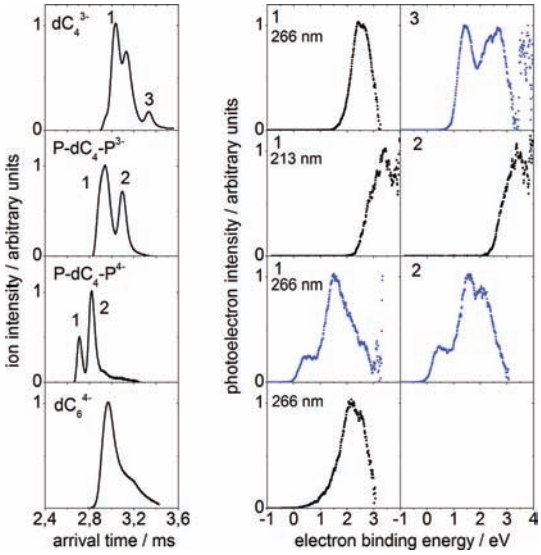

Figure 4. Comparison of the ATDs (left) and isomer resolved PES spectra (right) as obtained for dC$_4^{3-}$, for the P−dC$_4$−P derivative in its triply and quadruply charged/deprotonated state, and for dC$_6^{4-}$. Except for (P−dC$_4$−P)$^{3-}$, which was probed at a detachment wavelength of 213 nm, all other measurements were recorded at 266 nm. Blue curves highlight molecular ions with similar PES spectral structure, manifesting both a resolved low and a higher energy feature in contrast to the other multianions probed. Note that dC$_4^{3-}$(2), which has a PES spectrum very similar to dC$_4^{3-}$(1), is only shown in Figure 2 to save space.

In both charge states, the ATD indicates two different structures. To record PES spectra for each of the two (P−dC$_4$−P)$^{3-}$ isomers, it was necessary to use the fifth harmonic of the Nd:YAG laser (213 nm). We could not observe significant photodetachment of (P−dC$_4$−P)$^{3-}$ at 266 nm. PES spectra at 213 nm for both isomers (see Figure 4) look very similar to each other and show an onset around 2.3 eV. In comparison to dC$_4^{3-}$(1 and 2), we therefore find a shift of the ADE by about 0.5 eV to higher binding energies. Instead of three phosphate groups, there are now five different such groups in the derivatized molecule. Assuming phosphate localization, the most advantageous distribution of the three excess electrons for reducing Coulomb repulsion is to put them on the first, third, and fifth phosphate groups. As compared to dC$_4^{3-}$(1 and 2), this would cause a shift to higher electron binding energies roughly consistent with our observations, and arguing that (P−dC4−P)$^{3-}$ has no deprotonated nucleobases.

The PES spectra (obtained at 266 nm) of the two isomers of (P−dC$_4$−P)$^{4-}$ are essentially identical. However, comparing them to (P−dC$_4$−P)$^{3-}$, we find a qualitatively different spectral structure, implying a different type of excess electron localization. Instead, the (P−dC$_4$−P)$^{4-}$ and dC$_4^{3-}$(3) measurements appear related: all three PES spectra show resolved low and high energy features. Figure 4 also contains a PES spectrum for dC$_6^{4-}$ to aid comparison. This species (ADE ≈ 1.0 eV) has a significantly higher electron binding energy than (P−dC$_4$−P)$^{4-}$ (ADE ≈ 0.2 eV for both (1) and (2)) and in particular does not show the low energy shoulder of the latter. Note that dC$_6^{4-}$ may be thought of as having a desoxycytidine attached to both the first and the last phosphate groups of (P−dC$_4$−P)$^{4-}$. Assuming that dC$_6^{4-}$ consists of four (of a possible five) deprotonated phosphate groups, the significantly lower ADE measured for (P−dC$_4$−P)$^{4-}$ cannot be well reconciled with a completely phosphate-localized excess charge motif in the latter species too, suggesting at least one electron is localized elsewhere (in both isomers). Only base deprotonation is possible here as both terminal hydroxyl groups of dC$_4$ were "protected" to form P−dC$_4$−P. For completeness, we have also performed corresponding measurements on (P−dC$_4$−P)$^{5-}$ and display the results in the Supporting Information (Figure S3). A single isomer with a negative ADE of ∼ −1.0 eV is observed, as expected for a (P−dC$_4$−P)$^{4-}$ spectrum "Coulomb shifted" to lower electron binding energy by an additional negative charge (cf., eq 2).

4.1.3. IMS-PES of dN$_5^{4-}$ and dN$_6^{5-}$ (N = A, C, T, and G). Figure 5 shows ion mobility data and PES spectra (obtained at

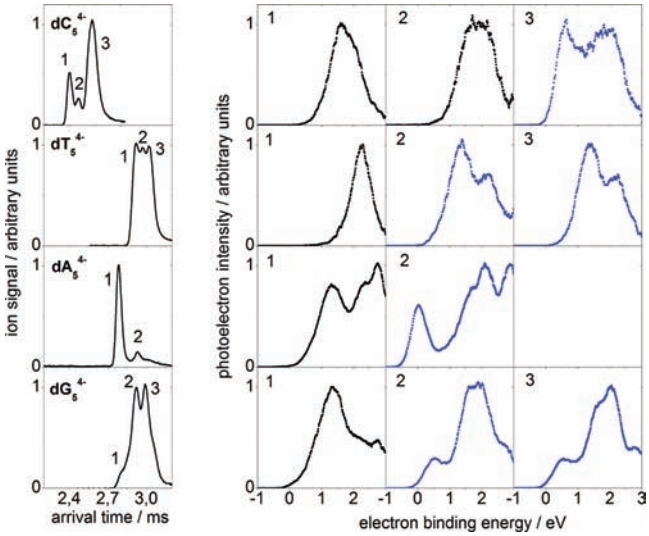

Figure 5. ATDs (left) and PES spectra (right) obtained at 266 nm for the quadruply charged pentanucleotides. Blue curves highlight isomers with significantly lower ADEs than observed for the other isomers of the same dN$_5^{4-}$. We assign the former to class B structures having at least one deprotonated base; see text.

266 nm) for 4-fold deprotonated, quadruply negatively charged pentanucleotides. The ATD of dC$_5^{4-}$ indicates three separable conformers. There are two kinds of corresponding PES spectra. A broad feature at an electron binding energy of around 1.8 eV is present in every spectrum. A second, more weakly bound feature at around 0.6 eV is only observed for dC$_5^{4-}$(3). The other examined ions dT$_5^{4-}$, dA$_5^{4-}$, and dG$_5^{4-}$ also manifest isomers with two different kinds of PES spectra, corresponding to more compact structures with higher ADEs and less compact structures with lower ADEs (differing from those of the higher ADE isomers by more than 0.5 eV in all cases). Note that pentanucleotides have only four phosphate groups, and as a result there is only one way of localizing the four excess charges on the phosphates. The observation of two significantly different types of PES spectra suggests that the situation is likely analogous to dC$_4^{3-}$ for which we have previously suggested that a second type of deprotonation motif must also be present: one base and x − 2 phosphates are deprotonated.

dx.doi.org/10.1021/ja300619j | J. Am. Chem. Soc. 2012, 134, 7830−7841

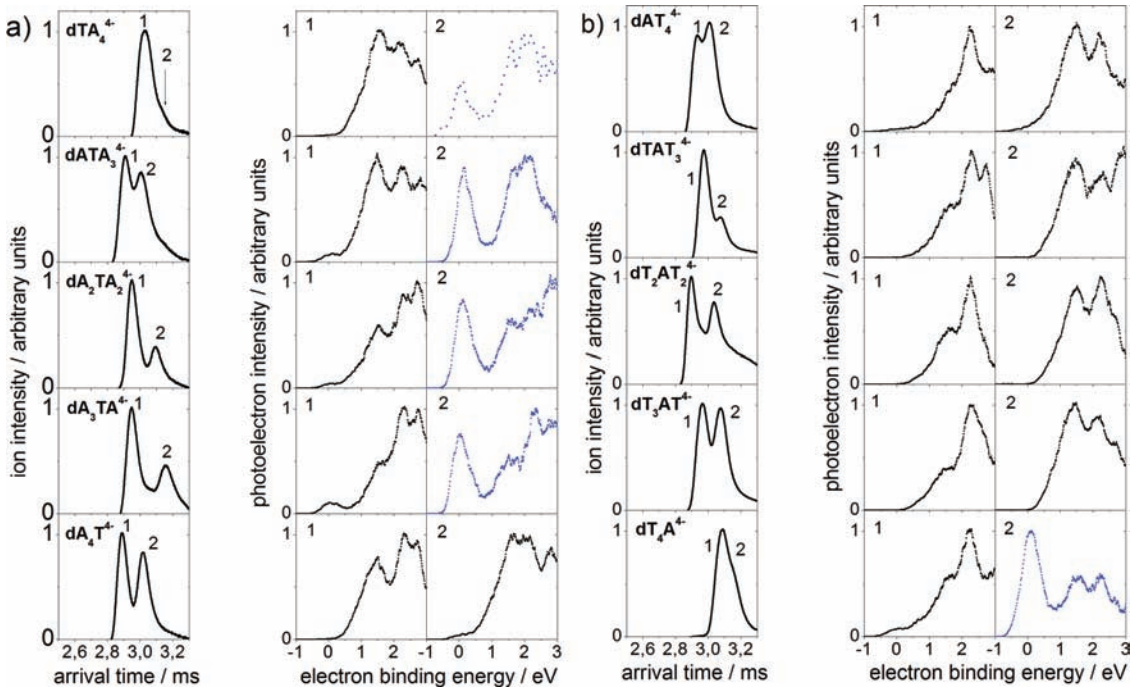

Figure 6. Arrival time distributions (ATD) and photoelectron spectra of quadruply charged pentanucleotides containing adenine and thymine. Blue curves indicate isomers assigned as having deprotonated bases. The dotted curve shown for dTA_4^{4-} was extracted from the poorly resolved ATD using the global fitting procedure outlined in ref 45.

We have also recorded the isomer-resolved PES spectra of all poly-N dN_6^{5-} (see Figure S4 in Supporting Information; the data for dC_6^{5-} have been previously published[45]). The trends are similar to those observed for dN_5^{4-}. Specifically, for dC_6^{5-} and dA_6^{5-}, we find relatively compact isomers having high ADEs together with less compact isomers with lower ADEs. Note the uncharacteristically wide range of collision cross sections observed for the four isomers of dC_6^{5-}. This leads to smaller differences between the ADEs of the two isomer classes than is observed for dT_6^{5-}. For dA_6^{5-}, only one (low ADE) isomer was obtained in measurable amounts. We assign both isomers resolved for dG_6^{5-} to the high ADE class; that is, no low ADE structure was observed for this oligonucleotide. Given the *x*-dependence of the ADEs observed for the "low ADE" isomers of the other $dN_x^{(x-1)-}$, N = C, A, and T, one would expect a corresponding dG_6^{5-} species to have an ADE significantly lower than −1.0 eV. While ADE ≈ −1.3 eV was still measurable for dA_6^{5-}, this was at the limit of our setup (see Experimental Methods). Conceivably, labile dG_6^{5-} species with an even lower ADE do not survive the transit time to the photoelectron spectrometer. As a corollary, analogous measurements of dN_7^{6-} were found to be problematic. On the other hand, preliminary IMS-PES measurements of poly-N dN_7^{5-} indicate that again two classes of isomer (having (i) low/high and (ii) high/low ADE/cross section, respectively) can be resolved, at somewhat lower overall charge density.

4.1.4. Sequence-Dependent IMS-PES of Mixed-Base Pentanucleotide Tetraanions. The experimental results for dC_4^{3-}, dN_5^{4-}, and dN_6^{5-} as well as the comparison of dN_5^{4-} measurements with semiempirical calculations (see below) suggest that nucleobases may be deprotonated in highly negatively charged gas-phase DNA oligonucleotides. If so, it is next of interest to consider whether specific base(s) in a given sequence might be preferentially deprotonated. We consider this issue for pentanucleotides, where the poly-N data sets show the clearest trends. With a peak maximum at an electron binding energy of ∼0 eV (see Figure 5), $dA_5^{4-}(2)$ has the lowest energy photodetachment feature seen among the "low ADE" dN_5^{4-} species. In contrast, $dT_5^{4-}(2/3)$ have the highest electron binding energies among their dN_5^{4-} isomer class. Therefore, deprotonated base isomers associated with a 5-mer sequence containing both adenine and thymine might be expected to show large differences in AEAs depending on whether adenine or thymine is deprotonated. We have therefore studied five different sequences of quadruply charged oligonucleotides containing a thymine and four adenines and vice versa. The corresponding measurements (ATDs and PES spectra) are shown in Figure 6.

For $dATA_3^{4-}$, $dA_2TA_2^{4-}$, and dA_3TA^{4-}, we find at least one isomer (2) for which a strong photoelectron signal appears around 0 eV. Consistent with the above argumentation chain, we assign this to a negatively charged, deprotonated adenine. The dotted PES spectrum $dTA_4^{4-}(2)$ was measured in the shoulder of the corresponding asymmetric ATD. It includes a signal around 0 eV, suggesting that a low intensity isomer comprising a deprotonated adenine also exists here. For dA_4T^{4-}, two distinguishable isomers are found. In the case of $dA_4T^{4-}(2)$, we observe a very weak signal around 0 eV, which might be due to a low intensity overlapping isomer having a deprotonated adenine.

The oligonucleotides containing four thymines and one adenine (see Figure 6) show the following behavior: dAT_4^{4-} has a bimodal, poorly resolved ATD with a weak photoelectron signal around 0 eV possibly present for the lower intensity isomer (1). dT_4A^{4-} shows an asymmetric ATD consisting of at least two different isomers. Taking a PES spectrum of the earlier part (1) of the ATD yields a weak band at 0 eV. This becomes much stronger if a PES spectrum is measured at the shoulder (2), implying that a deprotonated adenine is also present here. $dTAT_3^{4-}$, $dT_2AT_2^{4-}$, as well as dT_3AT^{4-} each

dx.doi.org/10.1021/ja300619j | J. Am. Chem. Soc. 2012, 134, 7830−7841

show two different well-separated structures. However, none of them gives rise to a PES spectrum with a measurable 0 eV feature, indicating that there are no deprotonated adenine isomers observable for these sequences.

To summarize, we observe isomers with a pronounced detachment feature at an electron binding energy around 0 eV for $dATA_3^{4-}$, $dA_2TA_2^{4-}$, dA_3TA^{4-}, dTA_4^{4-}, and dT_4A^{4-}. We attribute this to at least one deprotonated adenine. For dA_4T^{4-} as well as for dAT_4^{4-}, no definite conclusion could be drawn. Deprotonated adenine was definitely not seen for $dTAT_3^{4-}$, $dT_2AT_2^{4-}$, and dT_3AT^{4-}. This trend suggests that (adenine) base deprotonation preferentially occurs at either the first or in particular the last position of the sequence.

To provide further support for terminal base deprotonation, we have also examined a second binary pentanucleotide tetraanion permutation case. IMS-PES measurements obtained for five different sequences containing one guanine and four thymines (see Figure S5 in the Supporting Information) again show that a characteristic low binding energy feature is only observed if one of the two nucleobases, in this case guanine, is terminal.

4.2. Modeling the Charge Isomer Classes of dN_5^{4-}: Geometries and Energies. The experimentally determined collision cross sections and the corresponding experimental AEAs for all IM-resolvable isomers of dN_5^{4-} are summarized in Table 1, as derived from the measurements of Figure 5. We next discuss these results in terms of averages obtained from our semiempirical calculations for multiple trial geometries of the three different charge isomer types assumed, to check the plausibility of the tentative assignment made in the previous section. See section 3 and the schematic structures shown in Table 2 for an explanation of the charge isomer types A, B, and C. Two typical examples of actual molecular structures obtained using the AMBER + PM6 procedure are shown in Figure 7 for class A and B charge isomers of dA_5^{4-}.

Table 1. Experimentally Derived Collision Cross Sections (Ω_{exp}) and Adiabatic Electron Affinities (AEA_{exp}) for the Different IM-Resolvable Structures of the Quadruply Charged Homopentanucleotides in Order of Increasing Ω[a]

	Ω_{exp} [Å^2]/AEA_{exp} [eV]		
	isomer 1	isomers 2/3	
dC_5^{4-}	279/0.9	290/0.9	301/0.1
dT_5^{4-}	336/1.5	346/0.55	355/0.6
dA_5^{4-}	322/0.5	338/−0.4	
dG_5^{4-}	328/0.4	338/−0.1	347/−0.1

[a]See also Figure 5 and text.

Figure 8 plots PM6 total energies versus collision cross section for representative subsets of all dA_5^{4-} trial geometries, divided into charge isomer classes A, B, and C.

Using all of the trial geometries generated, we have calculated averages of the total and HOMO energies of all dN_5^{4-} species, for each of the three charge isomer classes. These are given in Table 2. Comparing the total energies, we infer that at the PM6 level, class A structures (i.e., fully deprotonated phosphates) are most favorable energetically. Beyond this, deprotonation of nucleic bases is found to more favorable than deprotonation of terminal hydroxyl groups. We also note from Table 2 that the negative HOMO binding energies of class B and C structures are generally significantly more negative than those of the fully phosphate deprotonated class A isomers.

Table 3 contains average geometric values for the lowest energy class A isomers. As compared to averages for B and C, A isomers are on average more compact, thus supporting our previous assignment of dN_5^{4-} isomers (1) to class A. For each N, Table 2 also presents the experimental AEA(1) value together with AEA(2/3)−AEA(1), that is, the difference between the AEAs of the isomers with the lowest and highest detachment thresholds, respectively. A comparison shows that AEA(2/3)−AEA(1) manifests roughly the same dependence on N as do HOMO(A)−HOMO(B) and HOMO(A)−HOMO(C), respectively. Therefore, on the basis of the PM6 HOMO binding energies alone, it is not possible to unequivocally assign the isomer-resolved PES spectra (2/3) to one of the two charge isomers (B) or (C). Nevertheless, the PM6 total energies of class B species are on average nearly 1 eV lower than those of class C, indicating that the former would be formed preferentially. Therefore, our model calculations support assignment of the low ADE isomers of dN_5^{4-} to class B.

4.3. Photodetachment Channels versus Charge Isomers. Next, we consider the underlying detachment mechanism, concentrating on the dN_5^{4-} system. As a first approximation, we model the threshold regions of the photoelectron spectra using eq 2 (and the photoelectric equation) and taking into account all energetically possible electron emission channels. We assume (i) electrons can be photoemitted from all subunits of a specific type (e.g., all phosphate groups) with equal probability if energetically allowed and (ii) these subunits are electronically decoupled from each other except for the "Coulomb field" due to the (other) localized excess charges. Comparing the predicted

Table 2. Average Values of the Total and HOMO Energies, Respectively, for Various Charge Isomers of the Quadruply Charged Pentanucleotides[a]

	E_{tot} (A)	E_{tot} (B)	E_{tot} (C)	E_{HOMO}(A)	E_{HOMO}(B)−E_{HOMO}(A)	E_{HOMO}(C)−E_{HOMO}(A)	AEA(1)	AEA(2/3) −AEA(1)
dC_5^{4-}	0	0.9	1.2	−2.5	−1	−0.1	0.9	−0.8
dT_5^{4-}	0	0.6	1.4	−3.1	−0.3	−0.8	1.5	−0.9
dA_5^{4-}	0	0.5	1	−2	−0.8	−0.4	0.5	−0.9
dG_5^{4-}	0	0.3	1.7	−2.3	−0.4	−0.3	0.4	−0.5

[a]In electronvolts, relative to the most stable reference isomers; see text for details. Calculations are based on three different localized charge motifs (A, B, and C) as indicated in the schematic drawing below the table. P_iH corresponds to a neutral, non-deprotonated phosphate. B_iH indicates a neutral and B_i^- a deprotonated base. 5-OH refers to a neutral hydroxyl group at the 5-end of the oligonucleotide, whereas 5-O^- indicates a deprotonated hydroxyl group. Also shown are experimental AEA values for the lowest (1) and highest (2/3) electron binding energy isomers (cf., Table 1).

dx.doi.org/10.1021/ja300619j | J. Am. Chem. Soc. 2012, 134, 7830−7841

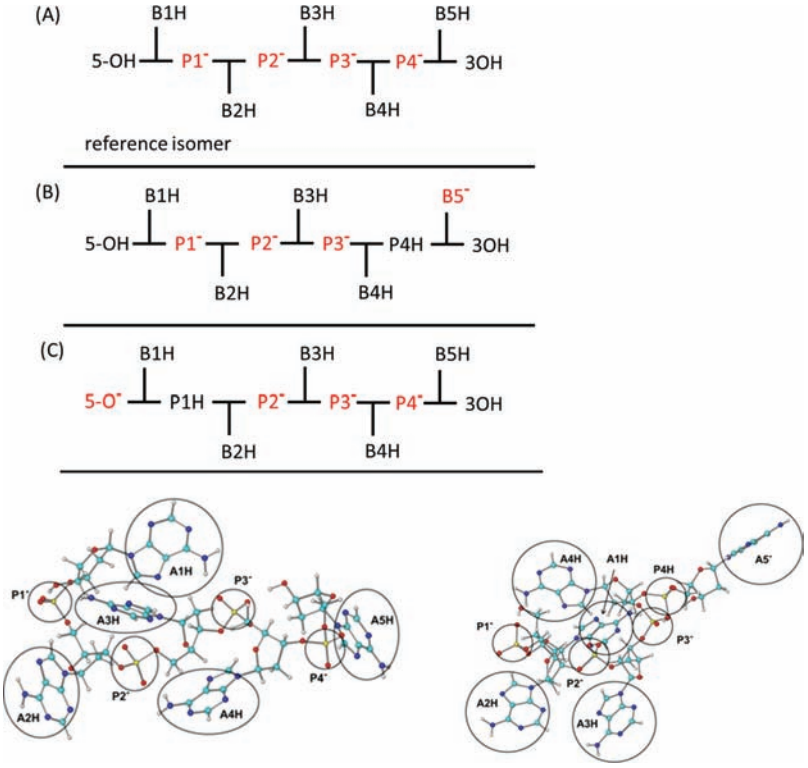

Figure 7. Typical low energy structures obtained from semiempirical calculations for each of the two isomer classes of dA_5^{4-}: class A isomer (left; note the fully deprotonated phosphates (P_i^-) and neutral adenines (A_iH)); and class B isomer (right; note the deprotonated adenine (A_5^-) and protonated phosphate (P_4H)).

electron kinetic energies with experiment then allows gauging which subunits are primarily responsible for the PES spectra.

Note that the strongly N-dependent experimental spectra obtained for dN_5^{4-} indicate that the repulsive Coulomb barrier (RCB) surfaces can be surmounted by the detachment photon energy in each case. Therefore, we do not need to explicitly take the RCB height into account to model the threshold regions of the PES spectra. In fact, the higher binding energy regions of our PES spectra can be analyzed to yield rough limits on the RCBs pertaining. For dN_5^{4-} isomers, we find values of ca. 2 eV consistent with an RCB height of 1.8(2) eV as previously reported for a dA_5^{4-} isomer mixture.[43] Note that these numbers are much smaller than the overall interetraanion Coulomb repulsion of 7−8 eV determined assuming four negative charges localized on the phosphate groups and an effective dielectric constant of one. However, one should bear in mind that the former value relates to removing an electron in the field of three residual (two-body) Coulomb interactions, whereas folding a 4− species together requires surmounting six separate repulsive interactions.

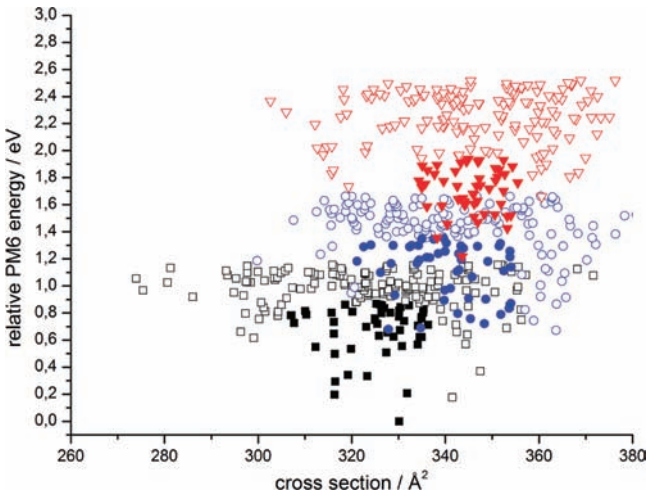

Figure 8. Representation of PM6 calculations as applied to dA_5^{4-} following procedures outlined in section 3. For each of three charge isomer types (black squares = class A; blue circles = class B; and red triangles = class C; see schematic in Table 2), we have generated 1000 structures by simulated annealing and have calculated their PM6 total energies and collision cross sections. We show here only 200 typical structures for each isomer type so as not to overload the figure. The best 50 structures (corresponding to the filled symbols) were used to determine the averaged total and HOMO energies as shown in Table 2 and discussed in section 3.

What are the energetically possible photodetachment channels? By analyzing the class A structures derived from PM6 calculations as discussed in section 4.2, we determine the average phosphate−phosphate distances in quadruply charged pentanucleotides to be quite similar independent of N (Table 3). Assuming that the detached electrons were (only) coming from the excess charges localized on the phosphate monoanions, we would therefore expect to see roughly the same ADE for each dN_5^{4-}. However, among the class A isomers of dN_4^{3-} and dN_5^{4-}, we observe a clear ordering of the electron binding energy: T > C > A ≈ G. Interestingly, the order of the experimentally determined VDEs of the neutral bases follows the same trend (see Table 3). So, it seems plausible, as was already suggested in refs 39, 44 for oligonucleotides with lower charge states (and charge densities), that the threshold electrons photodetached from class A isomers could be coming

dx.doi.org/10.1021/ja300619j | J. Am. Chem. Soc. 2012, 134, 7830−7841

Table 3. Averages of Calculated Collision Cross Sections and Distances between Deprotonated Phosphate Groups *i* and *j* (P_{ij}) for the Best Class A Structures of dN_5^{4-}[a]

	Ω_{calc} [Å^2]	P_{12}	P_{13}	P_{14}	P_{23}	P_{24}	P_{34}	AEA_{exp} [eV]	base	IP [eV]
dC_5^{4-}	295	6.1	11.2	16.7	6.8	11.7	7.0	0.9	C	8.9
dT_5^{4-}	340	6.2	12.9	18.7	7.3	13.1	6.3	1.5	T	9.2
dA_5^{4-}	324	6.7	11.9	17.6	7.2	12.2	6.6	0.5	A	8.4
dG_5^{4-}	327	6.5	12.1	18.1	7.0	11.9	7.4	0.4	G	8.0

[a]Calculations were performed according to procedures outlined in section 3. Also tabulated are experimentally determined adiabatic electron affinities (AEA_{exp}) for the IM-resolved structures assigned to class A isomers. Additionally, we list the ionization potentials of the neutral bases (IP). Note that AEA_{exp} and IP show a similar ordering (with base).

from neutral bases as well as from deprotonated phosphates. These two ionization mechanisms should also pertain to class B isomers. In addition, given our inference of deprotonated bases in the initial $(x - 1)^-$ species, we propose a third mechanism here: photodetachment from these deprotonated bases. Note that we can neglect ionization of neutral sugars (expected to have more strongly bound electrons[56]) and that we have already ruled out the possibility of deprotonated sugar hydroxyls being present above.

To test these three detachment channels further, we compare PES spectra predicted on their basis to experiment for dA_5^{4-}. The structural input for these electrostatic calculations comes from our semiempirical computations with which we have determined the best 50 plausible dA_5^{4-} candidate structures for each experimentally resolved collision cross section range (see also Figure 8, which plots the relative energies of representative structures versus their collision cross sections). PES spectral threshold contributions for each of the three possible detachment channels were calculated using eq 2. We have assumed a VDE of 5 eV for the phosphate monoanion groups,[57] 8.4 eV for the neutral adenine,[58] and 3 eV for detachment from the singly negatively charged deprotonated adenine.[41] Corresponding sums in eq 2 were over three other localized charges in the case of detachment from phosphate or deprotonated adenine. In the case of detachment from a neutral adenine, the sum is calculated over four localized charges. Such sums were calculated for each of the best 50 class A or class B structures, always taking into account (with equal weights) each of the discrete detachment sites corresponding to that specific detachment channel (e.g., electrons can derive from $P1^-$, $P2^-$, $P3^-$, and $P4^-$ for electron detachment from phosphates in class A). The results ordered according to these discrete detachment sites were then averaged over the 50 structures, and the resulting numbers were folded with Gaussian functions having widths chosen to result in bands comparable to those of the experimental spectrum. Figure 9 plots the resulting PES spectral prediction for the various detachment mechanisms.

In the case of class A structures, if electrons are removed from each of the four phosphate monoanion groups with equal probability, two electronic bands are predicted at 0.2 and 1.2 eV (denoted as P2/P3 and P1/P4, green curve), respectively. Note that detachment energies for phosphates located at the 5- and 3-ends are very similar. Similarly the second and the third phosphate groups have about the same VDE. If on the other hand the detached electrons are assumed to come from neutral adenines, the predicted PES spectrum more closely resembles the experiment. Conspicuous is the strong asymmetry between the 5- and 3-end, leading to local VDEs of 2.6 and 0.9 eV for A2 and A4, respectively (see schematic in Table 2 for numbering of the nucleobase sequence).

Note that our electrostatic model predicts a lower binding energy for phosphate detachment than actually measured. This implies either that there is significant electrostatic shielding of the excess charges (i.e., σ is not equal to one as assumed above) or that base photodetachment has a significantly larger cross section. Gabelica et al. have shown that the photodepletion cross sections of triply charged oligonucleotide hexamers are strongly correlated to the IP of the bases, implying that the effective cross section for photodetachment from neutral bases can be significantly larger than that for detachment from deprotonated phosphates.[39]

We now turn to class B structures, which we propose have a deprotonated terminal adenine A5 (and a neutral (protonated) P4). Here, we also obtain a better description of the experiment if we assume that electrons are directly detached from the adenine nucleobases (from neutral A1−A4 and from deprotonated A5) rather than from the phosphates. Note that the strong similarity between detachment energies for 5- and 3-terminal phosphates, which is predicted for class A species, is no longer observed for class B conformers. This is due to symmetry breaking when an adenine is deprotonated.

In closing, we note that a more realistic description of the experimental PE spectra should include phosphate, neutral base, and deprotonated base anion detachment in ratios corresponding to their actual photodetachment cross sections, which are presently unknown. Transitions yielding electronic excitations in both initial and final charge states (e.g., also delocalized excitations) as well the existence of other tautomers of the nucleic bases having different IPs also need to be taken into account.[59−61] Hopefully, our experimental results will stimulate appropriate higher-level theoretical descriptions of systems and detachment processes in future.

5. CONCLUSIONS

We have obtained isomer-resolved PES spectra of $dN_x^{(x-1)-}$, x = 4, 5, and 6. For all tetranucleotide trianions except for dC_4^{3-}, we found evidence for gas-phase structures in which exclusively the three phosphate groups are deprotonated, with corresponding localization of the excess negative charges thereon (class A). For dC_4^{3-}, all dN_5^{4-}, and most dN_6^{5-}, we also observed a second type of gas-phase isomer characterized by larger relative collision cross sections and comparatively lower VDEs (class B). We attribute these isomers to structures consisting of at least one deprotonated base (and ≤3 deprotonated phosphates). At room temperature and under collisionless conditions, class B charge isomers can coexist with fully deprotonated phosphate class A structures; that is, the two structure classes do not interconvert on the experimental time scale of ca. 1 ms. By permuting the sequence of bases in a variety of $[A_{5-x}T_x]^{4-}$ and $[GT_4]^{4-}$ pentanucleotides, we were also able to show that base deprotonation is most likely to

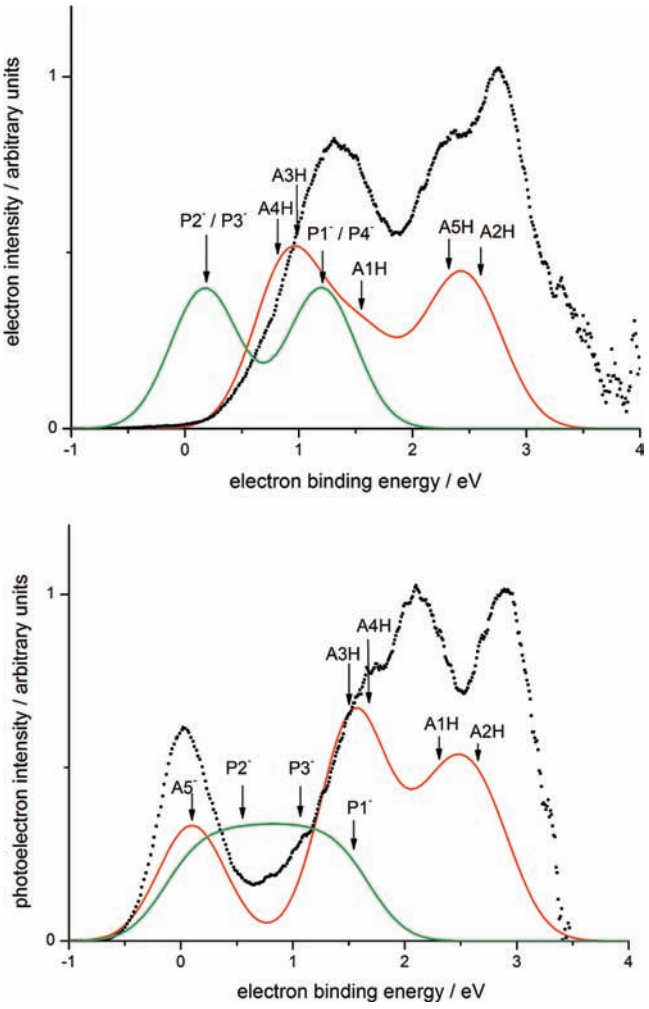

Figure 9. PES spectra of the two charge isomers of dA_5^{4-} in comparison to electrostatic model calculations based on three hypothetical photodetachment processes: (i) detachment from phosphates, (ii) detachment from neutral bases, and (iii) detachment from a deprotonated base. Shown in the top panel are predictions based on averaging over a representative set of class A structures (only deprotonated phosphates) versus the $dA_5^{4-}(1)$ measurement. Shown in the bottom panel are the corresponding predictions for class B structures (one deprotonated base) versus the $dA_5^{4-}(2)$ spectrum. See text for details on the calculations, which used structural input from PM6 calculations. Green curves indicate the range of predicted phosphate detachment energies. Red curves indicate base detachment energy range (note that "A5⁻" for the class B curve corresponds to detachment from the heterocyclic ring of the deprotonated adenine, whereas all other A_iH reflect detachment from neutral bases). P_i^- refers to the corresponding deprotonated phosphate group position i in the oligonucleotide sequence counting from the 5 end. Generally, the simulation is in better agreement with experiment for photodetachment from nucleobases rather than phosphates.

occur at terminal positions in the sequence. This behavior probably reflects the fact that such deprotonated-terminal-base charge isomers allow the overall Coulomb interaction between the excess charges to be reduced. Note that the abundance ratio of class B to class A structures can be increased by raising drift cell injection energies. This indicates that there must be "precursor geometries", which can unimolecularly transform to the corresponding class B isomers upon collisional excitation in the gas phase. In this sense, we can generate, kinetically "trap", and detect isomeric structures in the gas phase, which are not likely to be present in significant amounts in the original DNA oligonucleotide solutions before electrospraying.

UV irradiation of solvated DNA oligos[62,63] can lead to either excitation of individual bases or the formation of excitons delocalized over several stacked bases. Whereas excited nucleobases decay by ultrafast internal conversion, excitons live significantly longer and can eventually relax, for example, by photoluminescence. Gas-phase $dN_x^{(x-1)-}$ presumably manifest the same types of photoexcitation processes. Additionally, direct electron photodetachment is possible, albeit with a much smaller effective cross section than for resonant electronic excitation. Regarding the decay of resonant electronic excitations in isolated multianions, there are indications from studies on other systems[64] that electron tunneling autodetachment from electronically excited states can become appreciable on the time scales of photoelectron spectroscopy (ca. <100 ns), if competing decay channels are slow enough. Consequently, it is conceivable that the electrons being detected here derive not only from direct but also from such delayed photodetachment processes. Of course, also the electron kinetic energies resulting from delayed detachment must still conform to energy conservation; that is, the fastest electrons come from the most weakly electron binding sites/regions regardless of the detachment mechanism. Our experiments and calculations suggest that the bulk of the threshold photoelectrons derive from neutral and deprotonated bases.

In further PES of isomer-resolved $dN_x^{(x-1)-}$, it would be interesting to (i) systematically measure the dependence on detachment wavelength to differentiate delayed autodetachment from direct detachment features and (ii) perform pump−probe fsec-time-resolved photoelectron spectroscopy to learn about electron tunneling autodetachment rates (and exciton lifetimes). Also, more detailed geometric-structural information on the resolved isomers would be desirable, for example, by infrared multiphoton dissociation.[65,66] Analogous isomer-resolved PES experiments should also be performed on double-stranded DNA multianions. In the condensed phase, the stacked base motifs associated with the duplex structure are known to mediate both electron and hole delocalization.[67] In gas-phase isomers retaining double-helix structures, stacking-mediated delocalization would be expected to selectively stabilize the positive charge resulting from ionization of neutral bases (base-pairing precludes deprotonation). This should lead to changed detachment thresholds.

Here, we have probed minority $(x - 1)^-$ species not commonly investigated in ESI mass spectrometry studies of DNA oligonucleotides, which typically attempt to simulate the charge distributions present under physiological conditions. As a result, much lower relative charging levels with correspondingly more compact structures having effective sigma values significantly larger than one are generally encountered in the latter studies. On the other hand, the high excess charge states/charging levels used here allow (i) better exclusion of counterion complexation and (ii) shift the photoelectron spectra into an experimentally accessible detachment wavelength window (although, as the dG_6^{5-} measurement suggests, they can also be shifted too far). It turns out that these highly charged species can be intrinsically interesting in that among their resolvable isomers there are structures with both comparatively large collision cross sections and unusually low ADEs. We attribute these to species with one deprotonated base. If indeed they form via collisional activation of precursor structures, it seems unlikely that more than one base could be

dx.doi.org/10.1021/ja300619j | J. Am. Chem. Soc. 2012, 134, 7830−7841

deprotonated at a time, particularly for the short sequences studied here. While the relevance of such terminal deprotonated base structures to analytical mass spectrometry of DNA oligonucleotide multianions may be limited, base deprotonation of course occurs in aqueous DNA solutions at high alkaline pH's.[68] In the gas phase, such structures may be of further interest in the context of ion−molecule reactions leading to base modifications or as a route to novel modified surfaces/nanostructures by low energy ion beam deposition.

■ ASSOCIATED CONTENT

Supporting Information

High-resolution mass spectrum of the dA_5 sample; results of PM6 calculations for all 1000 class A trial structures of $dA5^{4-}$; ATD and corresponding PES spectrum obtained for the P-dC4-P derivative in its quintuply charged/deprotonated state; ATDs and corresponding PES spectra recorded at 266 nm for the quintuply charged hexanucleotides; and ATDs and PES spectra of quadruply charged pentanucleotides containing thymine and guanine.

This material is available free of charge via the Internet at http://pubs.acs.org.

■ AUTHOR INFORMATION

Corresponding Author

manfred.kappes@kit.edu

Notes

The authors declare no competing financial interest.

■ ACKNOWLEDGMENTS

This work was supported by the German Israeli Fund under collaborative grant number I-1029-12.5/2009. We thank our cooperation partner Ron Naaman for various stimulating discussions. Earlier support by the Deutsche Forschungsgemeinschaft for development of the IMS-PES apparatus is also gratefully acknowledged.

■ REFERENCES

(1) Hunt, D. F.; Hignite, C. E.; Biemann, K. *Biochem. Biophys. Res. Commun.* **1968**, *33*, 378.
(2) McNeal, C. J.; Ogilvie, K. K.; Theriault, N. Y.; Nemer, M. J. *J. Am. Chem. Soc.* **1982**, *104*, 976.
(3) Grotjahn, L.; Frank, R.; Blocker, H. *Nucleic Acids Res.* **1982**, *10*, 4671.
(4) Cerney, R. L.; Gross, M. L.; Grotjahn, L. C. *Anal. Biochem.* **1986**, *156*, 424.
(5) Covey, T. R.; Bonner, R. F.; Shushan, B. I.; Henion, J. D. *Rapid Commun. Mass Spectrom.* **1988**, *2*, 249.
(6) Hillenkamp, F.; Karas, M.; Ingendoh, A.; Stahal, B. In *Biological Mass Spectrometry*; Burlingame, A. L., McCloskey, J. A., Eds.; Elsevier: Amsterdam, 1990.
(7) Spengler, B.; Pan, Y.; Cotter, R. *Rapid Commun. Mass Spectrom.* **1990**, *4*, 99.
(8) Crain, P. F. *Mass Spectrom. Rev.* **1990**, *9*, 505.
(9) McLuckey, S. A.; Van Berkel, G. J.; Glish, G. L. *J. Am. Soc. Mass Spectrom.* **1992**, *3*, 60.
(10) McLuckey, S. A.; Habibi-Goudzrzi, S. *J. Am. Chem. Soc.* **1993**, *115*, 12085.
(11) Little, D. P.; Speir, J. P.; Senko, M. W.; O'Connor, P. B.; McLafferty, F. W. *Anal. Chem.* **1994**, *66*, 2809.
(12) Little, D. P.; Chorush, R. A.; Speir, J. P.; Senko, M. W.; Kelleher, N. L.; McLafferty, F. W. *J. Am. Chem. Soc.* **1994**, *116*, 4893.
(13) Little, D. P.; McLafferty, F. W. *J. Am. Chem. Soc.* **1995**, *117*, 6783.
(14) Christian, N. P.; Colby, S. M.; Giver, L.; Houston, C. T.; Arnold, R. J.; Ellington, A. D.; Reilly, J. P. *Rapid Commun. Mass Spectrom.* **1995**, *9*, 1061.
(15) Ni, J.; Pomerantz, S. C.; Rozenski, J.; Zhang, Y.; McCloskey, J. A. *Anal. Chem.* **1996**, *68*, 1989.
(16) Nelson, C. M.; Zhu, L.; Tang, W.; Smith, L. M.; Crellin, K.; Berry, J.; Beauchamp, J. L. *Proc. SPIE* **1996**, *2680*, 247.
(17) Gidden, J.; Bowers, M. T. *Eur. Phys. J. D* **2002**, *20*, 409.
(18) Gidden, J.; Bowers, M. T. *J. Phys. Chem. B* **2003**, *107*, 12829.
(19) Gidden, J.; Bowers, M. T. *J. Am. Soc. Mass Spectrom.* **2003**, *14*, 161.
(20) Hoaglund, C. S.; Liu, Y.; Ellington, A. D.; Pagel, M.; Clemmer, D. E. *J. Am. Chem. Soc.* **1997**, *119*, 9051.
(21) Gidden, J.; Ferzoco, A.; Baker, E. S.; Bowers, M. T. *J. Am. Chem. Soc.* **2004**, *126*, 15132.
(22) Gidden, J.; Baker, E. S.; Ferzoco, A.; Bowers, M. T. *Int. J. Mass Sectrom.* **2005**, *240*, 183.
(23) Baker, E.; Bowers, M. T. *J. Am. Soc. Mass Spectrom.* **2007**, *18*, 1188.
(24) Baker, E. S.; Dupuis, N. F.; Bowers, M. T. *J. Phys. Chem. B* **2009**, *113*, 1722.
(25) Smargiasso, N.; Rosu, F.; Hsia, W.; Colson, P.; Baker, E. S.; Bowers, M. T.; De Pauw, E.; Gabelica, V. *J. Am. Chem. Soc.* **2008**, *130*, 10208.
(26) Baker, E. S.; Bernstein, S. L.; Bowers, M. T. *J. Am. Soc. Mass Spectrom.* **2005**, *16*, 989.
(27) Rosu, F.; Gabelica, V.; Poncelet, H.; De Pauw, E. *Nucleic Acids Res.* **2010**, *38*, 5217.
(28) Gabelica, V.; Baker, E. S.; Teulade-Fichou, M.; De Pauw, E.; Bowers, M. T. *J. Am. Chem. Soc.* **2007**, *129*, 895.
(29) Collie, G. W.; Parkinson, G. N.; Neidle, S.; Rosu, F.; De Pauw, E.; Gabelica, V. *J. Am. Chem. Soc.* **2010**, *132*, 9328.
(30) Balbeur, D.; Widart, J.; Leyh, B.; Cravello, L.; De Pauw, E. *J. Am. Soc. Mass Spectrom.* **2008**, *19*, 938.
(31) Balbeur, D.; Dehareng, D.; De Pauw, E. *J. Am. Soc. Mass Spectrom.* **2007**, *18*, 1827.
(32) Balbeur, D.; Dehareng, D.; De Pauw, E. *J. Am. Soc. Mass Spectrom.* **2010**, *21*, 23.
(33) Schnier, P. D.; Klassen, J. S.; Strittmatter, E. F.; Williams, E. R. *J. Am. Chem. Soc.* **1998**, *120*, 9605.
(34) Klassen, J. S.; Schnier, P. D.; Williams, E. R. *J. Am. Soc. Mass Spectrom.* **1998**, *9*, 1117.
(35) Koeniger, S. L.; Merenbloom, S. I.; Valentine, S. J.; Jarrold, M. F.; Udseth, H. R.; Smith, R. D.; Clemmer, D. E. *Anal. Chem.* **2006**, *78*, 4161.
(36) Merenbloom, S. I.; Koeniger, S. L.; Valentine, S. J.; Plasencia, M. D.; Clemmer, D. E. *Anal. Chem.* **2006**, *78*, 2802.
(37) Lowery, K. A. S.; Hofstadler, S. A. *J. Am. Soc. Mass Spectrom.* **2003**, *14*, 825.
(38) Smith, S. I.; Brodbelt, J. S. *Anal. Chem.* **2010**, *82*, 7218.
(39) Gabelica, V.; Rosu, F.; Tabarin, T.; Kinet, C.; Antoine, R.; Broyer, M.; De Pauw, E.; Dugourd, P. *J. Am. Chem. Soc.* **2007**, *129*, 4706.
(40) Gabelica, V.; Rosu, F.; De Pauw, E.; Lemaire, J.; Gillet, J. C.; Poully, J. C.; Lecomte, F.; Gregoire, G.; Schermann, J. P.; Desfrancois, C. *J. Am. Chem. Soc.* **2008**, *130*, 1810.
(41) Chen, C. M.; Wiley, J. R.; Chen, E. S. *Nucleosides, Nucleotides Nucleic Acids* **2008**, *27*, 506.
(42) Lum, R. C.; Gabrowski, J. J. *J. Am. Chem. Soc.* **1992**, *113*, 8619.
(43) Weber, J. M.; Ioffe, I. N.; Berndt, K. M.; Löffler, D.; Friedrich, J.; Ehrler, O. T.; Danell, A. S.; Parks, J. H.; Kappes, M. M. *J. Am. Chem. Soc.* **2004**, *126*, 8585.
(44) Yang, X.; Wang, X. B.; Vorpagel, E. R.; Wang, L. S. *Proc. Natl. Acad. Sci. U.S.A.* **2004**, *101*, 17588.
(45) Vonderach, M.; Ehrler, O. T.; Weis, P.; Kappes, M. M. *Anal. Chem.* **2011**, *83*, 1108.
(46) Tang, K.; Shvartsburg, A. A.; Lee, H. N.; Prior, D. C.; Buschbach, M. A.; Li, F.; Tolmachev, A. V.; Anderson, G. A.; Smith, R. D. *Anal. Chem.* **2005**, *77*, 3330.

(47) Kruit, P.; Read, F. H. *J. Phys. E* **1983**, *16*, 313.
(48) Cheshnovsky, O.; Yang, S. H.; Pettiette, C. L.; Craycraft, M. J.; Smalley, R. E. *Rev. Sci. Instrum.* **1987**, *58*, 2131.
(49) Wang, X. B.; Wang, L. S. *Nature* **1999**, *400*, 245.
(50) Wang, X. B.; Ferris, K.; Wang, L. S. *J. Phys. Chem. A* **2000**, *104*, 25.
(51) Case, D. A.; Pearlman, D. A.; Caldwell, J. W.; Cheatham, T. E.; Wang, J.; Ross, W. S.; Simmerling, C. L.; Darden, T. A.; Merz, K. M.; Stanton, R. V.; Cheng, A. L.; Vincent, J. J.; Crowley, M.; Tsui, V.; Gohlke, H.; Radmer, R. J.; Duan, Y.; Pitera, J.; Massova, I.; Seibel, G. L.; Singh, U. C.; Weiner, P. K.; Kollman, P. A. *AMBER 7*; University of California: San Francisco, CA, 2002.
(52) Wyttenbach, T.; von Helden, G.; Batka, J. J.; Carlat, D.; Bowers, M. T. *J. Am. Soc. Mass Spectrom.* **1997**, *8*, 275.
(53) Wyttenbach, T.; Witt, M.; Bowers, M. T. *J. Am. Chem. Soc.* **2000**, *122*, 3458.
(54) Stewart, J. J. P. *J. Mol. Model.* **2007**, *13*, 1173.
(55) Wang, X. B.; Ferris, K.; Wang, L. S. *J. Phys. Chem. A* **2000**, *104*, 25.
(56) Kim, N. S.; LeBreton, P. R. *J. Am. Chem. Soc.* **1996**, *118*, 3694.
(57) Wang, X. B.; Vorpagel, E. R.; Yang, X.; Wang, L. S. *J. Phys. Chem. A* **2001**, *105*, 10468.
(58) Lin, J.; Yu, C.; Peng, S.; Akiyama, I.; Li, K.; Lee, L. K.; LeBreton, P. R. *J. Am. Chem. Soc.* **1980**, *102*, 4627.
(59) Li, X.; Bowen, K. H.; Haranczyk, M.; Bachorz, R. A.; Mazurkiewicz, K.; Rak, J.; Gutowski, M. *J. Chem. Phys.* **2007**, *127*, 174309.
(60) Haranczyk, M.; Gutowski, M.; Li, X.; Bowen, K. H. *Proc. Natl. Acad. Sci. U.S.A.* **2007**, *104*, 4804.
(61) Harańczyk, M.; Gutowski, M. *Angew. Chem., Int. Ed.* **2005**, *44*, 6585.
(62) Buchvarov, I.; Wang, Q.; Raytchev, M.; Trifonov, A.; Fiebig, T. *Proc. Natl. Acad. Sci. U.S.A.* **2007**, *104*, 4794.
(63) Takaya, T.; Su, C.; de La Harpe, K.; Crespo-Hernandez, C. E.; Kohler, B. *Proc. Natl. Acad. Sci. U.S.A.* **2008**, *105*, 10285.
(64) Ehrler, O. T.; Yang, J. P.; Sugiharto, A. B.; Unterreiner, A. N.; Kappes, M. M. *J. Chem. Phys.* **2007**, *127*, 184301.
(65) Stearns, J. A.; Mercier, S.; Seaiby, C.; Guidi, M.; Boyarkin, O. V.; Rizzo, T. R. *J. Am. Chem. Soc.* **2007**, *129*, 11814.
(66) Svendsen, A.; Lorenz, U. J.; Boyarkin, O. V.; Rizzo, T. R. *Rev. Sci. Instrum.* **2010**, *81*, 073107.
(67) Genereux, J. C.; Barton, J. K. *Chem. Rev.* **2010**, *110*, 1642.
(68) Franceschini, L.; Mikhailova, E.; Bayley, H.; Maglia, G. *Chem. Commun.* **2012**, *48*, 1520.